Detection in low target to clutter ratio by massive multilooking. Application to the recovery of engine fragments buried in Greenland icesheet

Hubert Cantalloube

Detection in low target to clutter ratio by massive multilooking. Application to the recovery of engine fragments buried in Greenland ice-sheet.

Hubert M.J. Cantalloube[a]

[a]ONERA Université Paris Saclay, F-91123 Palaiseau, France

Abstract

ONERA SAR system Sethi was involved in April 2018 in the search of engine fragments lost 6 months before by a jet-liner en route over Greenland and later buried under $\simeq$ 2m of snow. Their radar echoes were thus attenuated by the propagation through snow and, because of the high backscattering of the surrounding ice, the target to clutter ratio was below 10% at X-band. Though the icesheet clutter is very homogeneous, detection of such low contrasted targets requires a very high level of multilooking to yield significant detection at a false alarm rate compatible to the wide area covered.

1   Introduction

Following the loss of an engine fan assembly by a jet-liner above the Greenland ice-sheet [1],[2]&[3], ONERA had been approached for localising fragments that escaped optical detection from early explorations of the accident area and were critical for the accident cause investigation.

These fragments are heavy titanium parts of the fan hub that were expected to have penetrated to about 1 m inside the ice-sheet upon impact, and were soon covered with snow drift, concealing them from optical detection.

Ballistic computations from accident location, probable fragments ejection angle & velocity, drag coefficient and altitude wind estimations determined a wide ($\simeq$ 25 square km) search area for these fragments. ONERA proposed a multi-frequency SAR survey of this search area using the expected penetration of radio-waves in dry snow and/or ice.

This survey was performed in April 2018, 6 months after the accident, when an extra 1.5 m of snowfall covered the area. First processing of the acquired X, L and UHF band images did not yield any convincing hub fragment detection, because of the high clutter level and either low target cross-section at low bands or high target echo attenuation at high band.

However, further post-processing showed that a fan hub part intentionally buried 1.2 m depth close to the search area can be detected at X-band but with a very poor target to clutter ratio (the fragment echo was only 10% of the clutter level in the same pixel).

This low target contrast (20 dB *below* the clutter) is two order below the generally assumed contrast requirement for a radar detection (as a rule of thumb, a contrast of 13 dB *above* the clutter is a frequent assumption). This high contrast requirement is due to the fact that clutter level is an *average* value, and due to speckle individual pixel measure values are dispersed with a standard deviation of approx-

imatively half of this average, thus roughly 30% of the clutter pixel value of a radar image are above the expected level at the target (the 13 dB rule corresponds to about 2 pixels per billion above the expected level at target).

In order to reliably detect the searched fragments with a sensible false alarm rate, we needed to reduce speckle fluctuations of the clutter well below the target level, hence massively multilook the image (typically an equivalent number of look of 100 at least was required). This was possible because we could compute several independent looks for each polar channel of each acquisitions, and that our acquisition plan involved several headings and several incidence angles (and sometimes revisit with InSAR processing objectives).

This paper describes the SAR post-processing issues for computing massive multilook images focused below surface in a slowly drifting, high backscattering, non Lambertian environment.

1.1   Motivation for massive multilooking

The search area was approximately 5 by 5 km wide, and any false alarm investigation has an high cost: just after acquisition, digging at one alarm required shovelling some two tons of snow, and eventual fragment recovery, 21 months after accident, required to dig some 16 m^3 of snow (and marginally cross two 10 cm thick ice layers with a chainsaw). Such an operation in an hostile polar high (1850 m) altitude environment is a very demanding task for highly trained polar explorers.

To understand the challenge of fragment detection, at X-band (20 cm resolution), our search area is 6 10^8 pixels, our target has a diameter below 4 pixels (the full hub diameter is 80 cm). Target echo adds 10% to the clutter return, hence for a single look, any threshold on the image would yield high non detection rate and/or high false alarm rate (**Figure 1**).

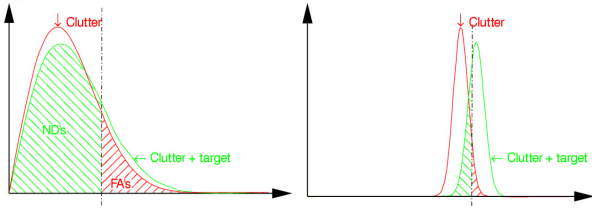Due to the small target size, space multilooking (averag-

Figure 1 Comparison of pixels level density function for clutter only in red and clutter + target in green for single look (left) and 18 equivalent looks (right). For a given threshold, non detections are figured by the green area and false alarms by the red area.

ing of nearby pixels) beyond 12 equivalent looks (ENL) will surely dilute the target signal. Pixel level density on Figure 1-right (18 ENL) corresponds to the span (sum of all polar channels) of 6 sub-aperture images from one single X-band acquisition (and more or less to that of the maximum space multilooking of a single look image). Of course, because the red area is visible on the figure 1, it is much higher than the 10^{-8} to 10^{-7} range sensible FA rate. For example, the **Figure 2** show the image and its histogram around the test-fragment (only 40% of the size of the eventually recovered fragment) that was buried by the first GEUS expedition. The top row correspond to one acquisition (24 looks), the middle one to the 3 acquisitions of one heading (72 looks) and the bottom one to all acquisitions (432 looks). The vertical red line on the histogram indicates the target RCS value. For rendition, the dynamic of the images are clipped between 90 an 110% of the clutter level.

1.2 Technical difficulties for massive multi-looking

The eventual extend of the target on the image is not exactly known: fragment is *part* of a 80 cm diameter hub, hence may be smaller, however, the amount of smearing of the target due to blurring by the overlaid snow/ice irregularities is unknown. Therefore, we choose to make a full resolution multilook image (i.e. without space averaging) from all available acquisitions at X-band and later add space multilooking from the size of the structuring element (SE) for the "top-hat" constant false alarm rate filter (CFAR). We tested 3, 5 and 7 pixels for the SE diameter (54 to 126 cm).

Since we can make 6 sub-aperture images at the 20 cm resolution per acquisition channel, and we have 4 polar channels. Each acquisitions yields 24 single look images (with an ENL of only 18 because of the reciprocity "law" that makes the cross-channels Hv & Vh similar).

Four headings (parallel & perpendicular to the accidented plane trajectory) were acquired at X-band, each heading was acquired as three parallel sub-swathes with 2/3 overlap between adjacent subswathes. Parallel headings were acquired with 30° antenna depression. Perpendicular headings were acquired twice (with InSAR application in mind) with 50° antenna depression. Thus the total number of acquisition was 18, yielding a grand total of 432 single look
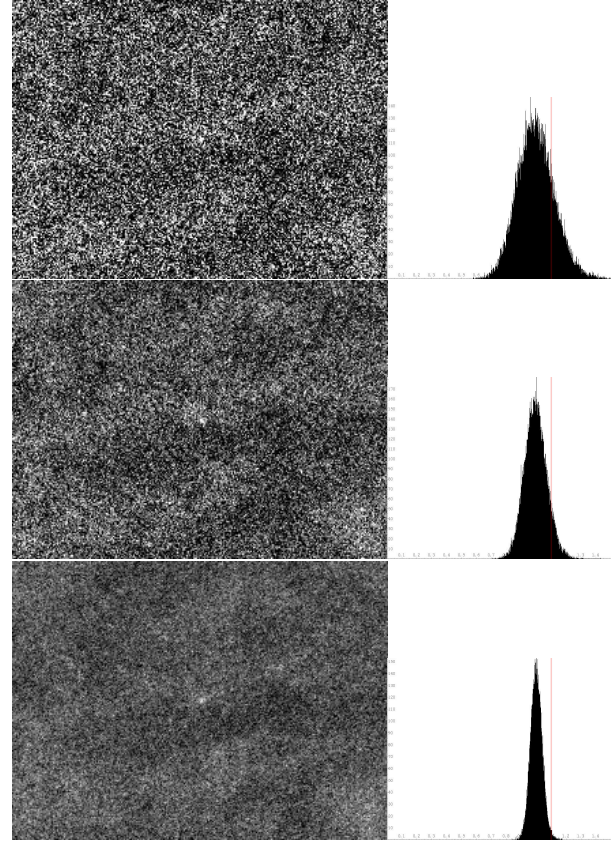

Figure 2 Comparison of image and measured histogram around a test-fragment buried on site (the bright spot at the middle). Top 24-look image, middle 72-look image, bottom 432 look image.

images to fuse.

The fusion law for minimising speckle is relatively straightforwards[4] and depends of the respective signal to noise ration (SNR). The weights of each component should be proportional to $\frac{SNR}{SNR+1}$, with the SNR being understood as "clutter to noise" ratio. The only extra twist here is that the two corresponding cross-pol channels must be added prior to combining yielding a 3dB SNR increase.

Besides the computer issues of synthesising, mapping to ground coordinate and store 432 images & ancillary data of 25 000×25 000 pixels each, the main difficulties arise from the registration of the images (when from different acquisition) and SNR evaluation.

1.2.1 (Absolute) image registration issues

First, we could not rely on some tie-point to register images from distinct acquisitions, because the search area is extremely homogeneous, and the calibrator that was setup for that purpose at the edge of the search zone two weeks prior to our campaign by a polar expedition of GEUS (A zenith looking Luneburg sphere) ended up covered with snow in the middle of our campaign.

Fortunately, our dGPS hybridized inertial navigation unit (INU) provides a trajectory of high accuracy (10 cm horizontal and 20 cm vertical nominally) which allows 10 cm azimuth resolution at 5 km range without any autofocus. Since we have a reinjection of the transmitted pulse

recorded together with the radar signal (and also a "noise" window) we can calibrate the possible drift of the radar internal delays to a fraction of ns. This results in an absolute image registration accuracy within 50 cm without any tie-point (worst case estimate from limit AF-less resolution and absolute INU accuracy is 135 cm , but errors measured on landmarks such as geodetic points show the real accuracy is better than the worst case derived form the nominal error values).

Of course, this assumes that the terrain altitude is known. In our context, the DTM for the surface was obtained from the Icesat mission. The DTM was locally debiased by few surface accurate GPS measures made during the GEUS setup expedition and by several vertical SAR surface altimetric profiles.

However, our targets were not at the surface, but buried under 1 to 3 m of snow/ice, with an unknown refractive index (but typically 1.25 to 1.35 in the first few m).

1.2.2 Registration depth issues

Though actual target depth was then unknown (since its recovery, we now know that the top of the bigger fragment was 1.8 below the surface during SAR acquisitions) we had the opportunity to observe some other not recovered salient engine fragments such as the one on **figure 3** that we could assume to lie at comparable depth (eventually they were actually some 0.3 m higher).

Figure 3 Most salient engine fragment left on site (a cowling part) as visible from the surface 5 days after fall-out (and already partially covered by snowdrift). And from the Sethi radar at X-band 6 months after fallout (then covered by 1.5 m of snow/ice).

Numerical simulation with modelling the overlaid layer as a constant index homogeneous media showed that for the 30° antenna depression geometry, the effect of refraction on a target corresponds within a pixel to an offset in altitude (an apparent depth) in a media of index 1. Hence for these acquisitions, we can measure the "apparent" depth (stereo measurement) when matching salient fragments form opposite headings, and register the images biasing the DTM by the apparent depth.

For the 50° antenna depression geometry, the incidence angle varies more within the swath, yielding at the swath edges both a vertical offset "apparent depth" but also an horizontal offset slightly higher than a pixel. However, this occurs at the edge of the swath, where at steeper incidence the antenna illumination is low (at steeper incidence, antenna pattern yield a narrower footprint) hence we assumed the corresponding image would be weighted very low and the impact of the slightly out of bounds horizontal offset

on the overall target smearing could be neglected.

In conclusion, we measured two "apparent depths" for each of the two antenna depression values on salient known fragments and used them to register all images.

1.2.3 Surface motion issue

The images at X-band were acquired during two flights 5 days apart. The slow ice-sheet drift towards ocean, approximated to 60 m/yr at a global scale from space measurements, would correspond to a significant 4 pixel mismatch. Comparison of calibrating targets position measured at setup with the positions measured 13 and 18 days later from our SAR images are consistent with the large scale values, but show a stronger than expected gradient of ice drift velocity with longitude (60 m/yr at the fan fragment burial point, but 100 m/yr at the Luneburg lens). This strong gradient is corroborated by the dense North/South crevasse mesh, probably shear fractures as the velocity difference exceeds the ice plasticity limit (25 m/yr).

For our multilooking, the second flight was just offset by the average measured drift, the remaining deviation from this average amounting to about 1 pixel at most.

1.2.4 SNR (noise & clutter) evaluation issues

Once geometrically registered, the optimal combination of single look images depends on the SNR. The accurate evaluation of the SNR requires both a good evaluation of the noise level (mainly thermal noise) and clutter level. For this Greenland signal reprocessing, we updated our SAR processor to provide an extra ancillary output which is the thermal noise on the image computed from the input noise power density function (noise PDF) and the actual processing of the raw signal (including band equalisation, antenna pattern compensation, processing gain a.s.o.). The noise PDF itself is computed from noise samples measured after each transmitted pulse in a short receive window before the start of the nadir echo.

Clutter level is critical both for optimal weighting of images with varied SNR, but also to normalise the clutter variations with incidence angle that otherwise induce level discontinuities at the edges of the individual images in the final multilook image (**Figure 4**).

The clutter level variation with incidence was modelled for each polarisation by fitting a second degree curve to the level versus incidence angle scatter plot.

This clutter model is used for combining all 432 images into a search composite. Four partial composites corresponding to each acquisition heading are also computed for further target depth assessment.

2 Results

Target detection is performed by a "top-hat" CFAR filter on the final composite image, with a threshold slightly below the level at the fan part buried by the GEUS polar expedition. Filter SE diameter of 3, 5 and 7 were tested for accommodating the uncertainties on both actual target (fragment) size and target image blur by ice cover heterogeneity.
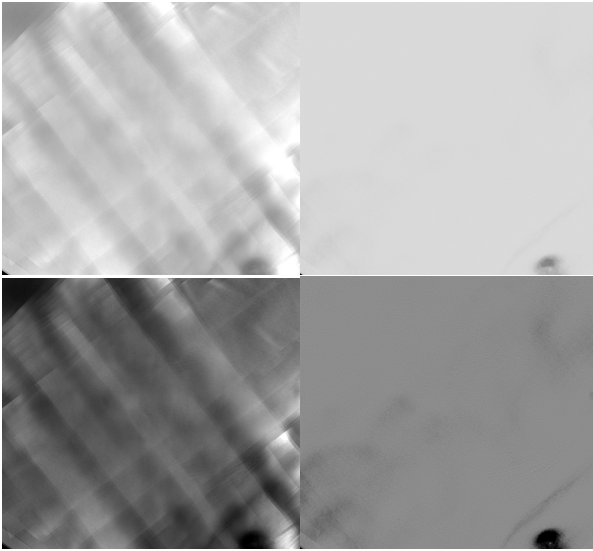
Figure 4 432 looks X-band composite assuming Lambertian clutter (left), and with the degree 2 clutter model (right). Top row images are with native dynamics, and bottom row images have contrast enhanced.
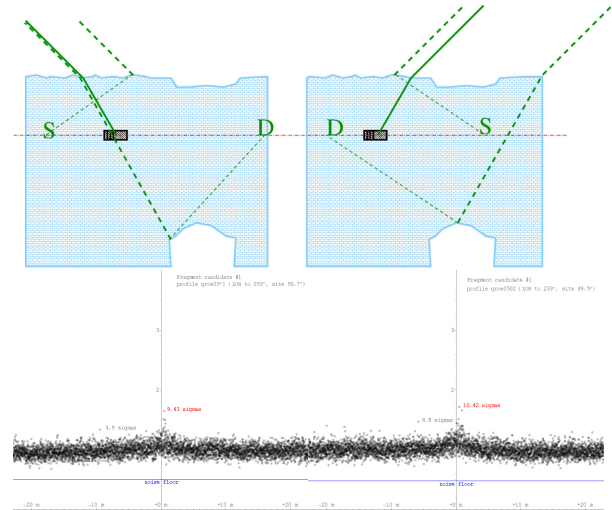

Figure 5 (Bottom) Comparison of candidate fragment X-band profiles from opposed heading confirming a depth close to that of known salient fragments. (Top) Surface or deeper echoes would appear offset (S and D marks) on the images registered to the salient fragment depth (red mixed line).

This yielded a hundred of target candidates, that were each individually examined:

First, alarms that appear just on a crevasse lip are discarded. This is not as straightforwards as it may seem, because depending on the position in the search area, the depth of the crevasse lips may differ significantly from the focus depth (the "snow bridge" above the crevasse may be thicker or thinner than the focus depth). Depth difference may cause the crevasse lips to overlay the target position. Here, the visibility of the target from different heading and comparison with crevasse lips positions allows to keep target candidates close but not at crevasse lips. This point proven important: the recovered hub fragment was just 1 m on the side of a crevasse with the snow bridge ending just 2 m below (a configuration that made the recovery challenging [3], **[5]**).

Second, target whose position variation between the heading was not consistent with the expected target depth were also discarded (**Figure 5**).

On this figure 5, the pixel values for the 72-look images obtained for opposed incident angles of 60° are plotted along range, the clutter level fluctuation correspond to the remaining speckle at an ENL of $\simeq$50, the blue line indicates the thermal noise level, and the deviation wrt clutter standard deviation is indicated for the target peak (in red) and the maximum off-target value (in black). The target peak position (+1 m) match between the two plots indication a target at the expected apparent depth. And both peak values are statistically significant (though the detection of this candidate was done on the full 432-look image, and not on each 72 or 144 looks "directional" images).

Note that both peaks are smeared to a width of slightly more than one meter (probably the ice/snow heterogeneity blurs the fragment image). Note also the shallow deep of the clutter at around +6–+7 m on the left plot and at +4–+5 m on the right plot corresponding to the nearby

crevasse air bubble (its position does not match because the air bubble top is $\simeq$4 m below the target depth.

2.1 Results at X-band: hub fragment(s) detection

At this stage, only one candidate remained (**Figure 6**). It was a point with level 21% above the clutter (twice brighter than the fan hub part buried for our training by the GEUS polar expedition). Due to its position in a dense crevasse field (the darker line south of the target, mostly visible on the contrast enhanced version, is the air bubble of a nearby crevasse), we were asked to provide "spare" candidates by relaxing our criteria. We provided two "spare" secondary candidates by lowering the filter threshold to just above the first sure false alarm. Sure false alarm are known because between the first unsuccessful processing and the reprocessing, a GEUS expedition, exhaustively scanned (during 3 weeks) with GPR some 5% of the search area, thus with a good confidence, any alarm within this scanned area should be a false alarm (**Figure 7**).

The final result of the detection was the accurate coordinates of the three targets (the main and the two spares) and seven unknown fragments that due to their downwind position are probably not heavy fan hub fragments. In order to translate these coordinates at the date of the airborne survey (images were registered to April 6th) to coordinate at the surface during the recovery expedition, we also provided the accurate coordinates of two targets from the setup at the same date. The instructions was to recover these setup target (there were marked with flags when setup) and use the offset between their present position and their remote detected one to derive the actual present position of the fan hub candidate targets. (On Figure 7 –reduced to 4×4 m pixel for fulfilling filesize limit–, there is a small offset between the blue cross-hair mark and the yellow cir-

Figure 6 Candidate for fan hub fragment on the final X-band image (left). On top the genuine image and at bottom the contrast is strongly emphasised. The dark horizontal line is a crevasse under 6 m snow-bridge. Recovery of the hub fragment 15 months after radar acquisition (right). The trench is about 4 m deep, the crevasse is ahead (photographer stands on the south lip of the trench).
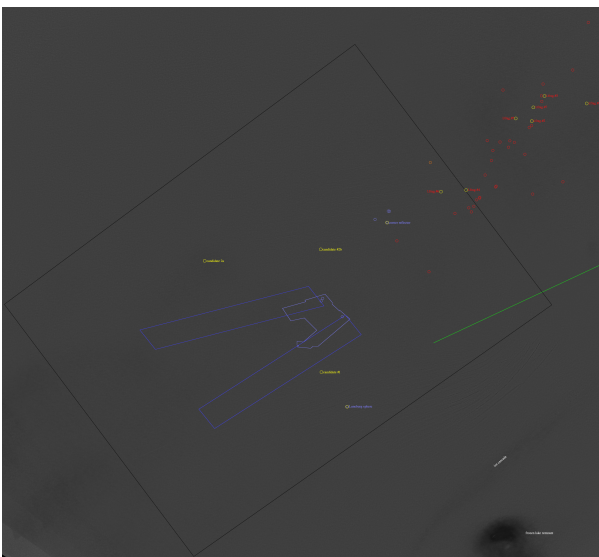

Figure 7 Final result of the airborne search campaign with the main and two spare targets (yellow circle with yellow label), seven salient fragments in the downwind fragment plume (yellow circle with red label), two buried targets for ice drift assessment (yellow circle with blue label). For reference, aircraft trajectory prior to engine fan explosion is in green, most probable hub fragment fallout zone in blue, known fragment location in red (without label, orange one is the fragment of figure 3), light blue area is the GPR scanned area and the blue circle the ice lens (false alarms) excavated during this expedition

cle at the setup targets, the former being at the coordinates of the target at setup, the latter being at the detected position 2 weeks later.)

2.2 results at L & UHF bands

During the preparation of the recovery expeditions, the L and UHF band signals have also been reprocessed using the same approach as X-band.
Contrast of the result at L-band was too low for efficiently

detecting targets, however the X-band candidates can be evaluated: The main candidate was visible at L band, but none of the "spare" candidates was visible (**Figure 8**).
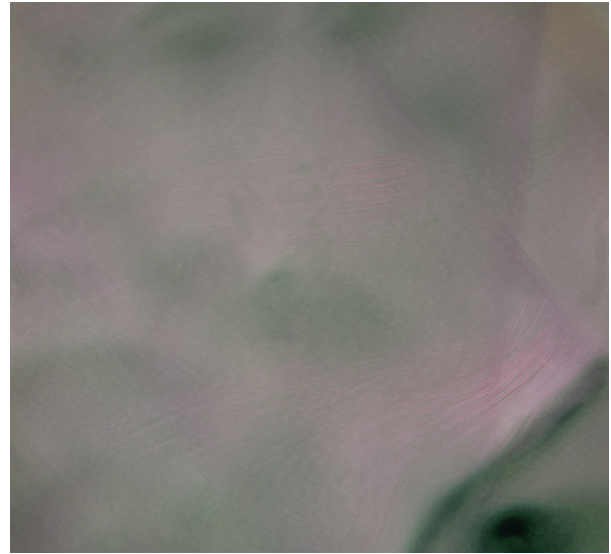

Figure 8 Composite of all L-band images on the same footprint as Figure 2. Polarisation is colour-coded red=cross, green=horizontal & blue=vertical.

Reprocessing at UHF band, though interesting in localisation of the crevasses around target, showed that no target (primary nor spares) are visible. Even the most salient fragment (the cowling part) is barely visible. However, UHF measure proven critical to hub fragment recovery: Due to deeper penetration, crevasses are much more efficiently detected at UHF band. Instead of focusing the UHF images at the target depth, we also focused the set at a depth of 30 m which is the depth of all crevasses bottom (below that depth, due to pressure, ice becomes plastic and crevasses wall merge **Figure 9**) Thus on the image focused at this depth, the bottom edges are in superposition for all observation directions emphasising the crevasses positions. The comprehensive map of crevasses derived from this UHF image allowed planning the helicopter landing in the narrow safe terrain between crevasses for recovery camp installation.

3 Conclusion & perspective

Six month after the candidate detection on the reprocessed images (15 months after the SAR acquisition campaign, 20 months after the accident) a GEUS polar expedition confirmed the main candidate with a TEM sensor (metal detector) 100 m downstream the ice flow. Only one of the setup target have been retrieved as the flags on the target setup were blown away. Unfortunately, the one closest to the main target candidate, the Luneburg lens (which is mostly composed of dielectric material) was undetectable with the TEM sensor. However, using the drift measured further away, the TEM sensor detected a significant target response at first try (the sensor was afterwards moved a few meters until the maximum signal was obtained).
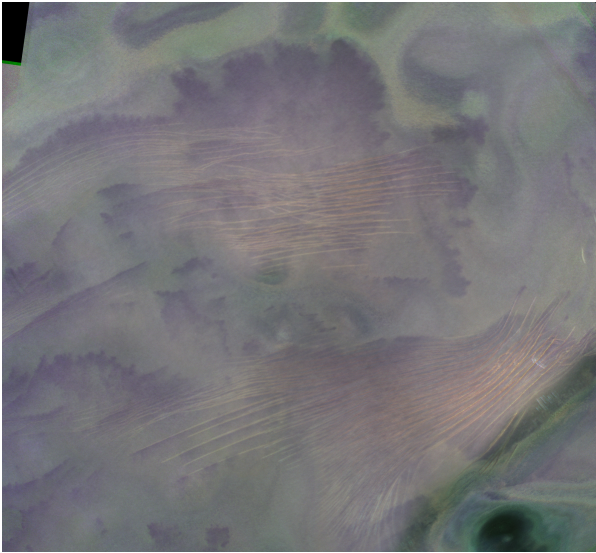
Figure 9 Composite of all UHF-band images focused at 30 m depth, thus emphasising the crevasses in the search zone. Polarisation is colour-coded red=cross, green=horizontal & blue=vertical.

The fragment (more than half of the hub with 9 severed blades still attached) was later recovered under 3.3 m of snow & ice. Its analysis by the engine manufacturer yielded an unexpected discovery: The widely used Ti-6Al-4V alloy that was previously thought to be insensitive to the fatigue dwell fracture mechanism failed on this fan hub at a macro-zone under a fan blade attachment slot from this very mechanism. An update of the periodical maintenance plan was issued by the engine manufacturer that should avoid any recurrence of this accident cause. Furthermore, future aircraft and engine design using Ti-6-4 alloy should implement wider structural margins against fatigue dwell failure.

The experience we have learned from this campaign could also prove useful in planning future SAR search for aircraft fragments in polar areas that are likely to occur with the growing air traffic in the polar routes beween Europe, North America & Asia.
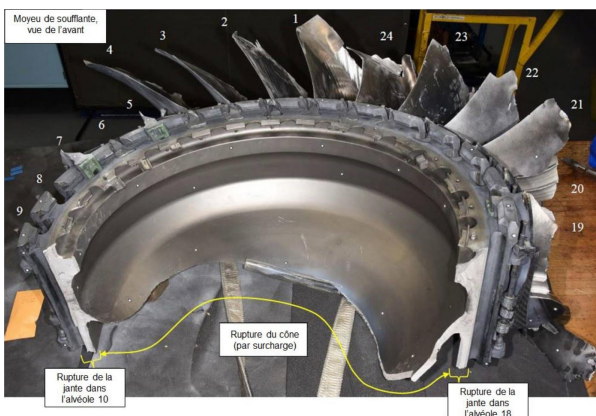

Figure 10 The recovered fan hub fragment with 9 fan blade fragments still attached (source French BEA).

5 Literature

[1] Bureau d'Enquêtes et d'Analyses (Stéphane OTIN): Technical Report, Accident to the Airbus A380 registered F-HPJE and operated by Air France on 30/09/2017 en route over Greenland October 2017 - June 2018 Searches Phase I & II, https://www.bea.aero/fileadmin/uploads/tx_elyextendttnews/F-HPJE_TECHNICAL_REPORT_11.pdf, Jun. 2019

[2] Bureau d'Enquêtes et d'Analyses (Stéphane OTIN): Technical Report, Accident to the Airbus A380 registered F-HPJE and operated by Air France on 30/09/2017 en route over Greenland June 2018 - June 2019 Phase III field campaign and part extraction, https://www.bea.aero/fileadmin/uploads/tx_elyextendttnews/F-HPJE_Phase_III_PUBLICATION_June_2020_08.pdf Jun. 2020

[3] Bureau d'Enquêtes et d'Analyses (Stéphane OTIN, *in French*): Rapport d'Enquête, accident de l'avion AIRBUS A380-861 équipé de moteurs Engine Alliance GP7270 immatriculé F-HPJE exploité par Air France survenu le 30 septembre 2017 en croisière au-dessus du Groenland (Danemark) BEA2017-0568 https://www.bea.aero/fileadmin/uploads/tx_elydbrapports/BEA2017-0568.pdf, Sep. 2020

[4] Cantalloube, H.; Nahum, C.: How to compute a multi-look SAR image?, CEOS SAR Workshop, ESA special publications Vol. 450, 2000, pp. 635-640

[5] Mankoff, K. et al.: Search and recovery of aircraft parts in ice sheet crevasse fields using airborne and in-situ geophysical sensors. J. of Glaciology 66(257), pp. 496-508. doi:10.1017/jog.2020.26, June 2020.